Separation and Purification Technology 76 (2010) 206–214

Contents lists available at ScienceDirect

Separation and Purification Technology

journal homepage: www.elsevier.com/locate/seppur

Catalytic hydrodechlorination of chlorophenols by Pd/Fe nanoparticles: Comparisons with other bimetallic systems, kinetics and mechanism

Tao Zhou[a,b], Yaozhong Li[c], Teik-Thye Lim[a,*]

[a] School of Civil and Environmental Engineering, Nanyang Technological University, 50 Nanyang Avenue, Singapore 639798, Republic of Singapore
[b] DHI-NTU Water & Environment Research Centre and Education Hub, Singapore 639798, Republic of Singapore
[c] Institute of Environmental Science and Engineering, Nanyang Technological University, Singapore 637723, Republic of Singapore

ARTICLE INFO

Article history:
Received 26 August 2010
Received in revised form 6 October 2010
Accepted 14 October 2010

Keywords:
Hydrodechlorination
Zerovalent iron
Nanoparticles
Chlorophenols (CPs)
Palladium

ABSTRACT

This study investigated dechlorination of 4-chlorophenol (4CP), 2,4-dichlorophenol (24DCP), and 2,4,6-trichlorophenol (246TCP) with Pd/Fe nanoparticles. The reaction rates were significantly faster than those achieved with Pt/Fe, Ni/Fe, Cu/Fe and Co/Fe nanoparticles. The chlorophenols (CPs) could be completely reduced to phenol by Pd/Fe following the pseudo-first-order kinetics, and the rates followed the order of 246TCP < 24DCP < 4CP. The 246TCP reduction rate with Pd/Fe increased with temperature and the estimated activation energy was 29.8 kJ/mol. The CPs dechlorination rate increased linearly with Pd loading, suggesting that Pd catalyst could be the only reactive site. Based on rigorous analysis of the transient formations and concentrations of various intermediates, a scheme of transformation pathways and the reaction mechanism was proposed to delineate 246TCP dechlorination to phenol. The influence of pH on the CPs dechlorination was investigated, and weak acidic condition is more favorable to the dechlorination reaction. H_2 evolution or iron corrosion rate initially followed the pseudo-first-order kinetics, and was reverted to the zero-order kinetics for prolonged reaction (>24 h).

1. Introduction

Zero-valent iron (ZVI) has been used successfully in the treatment of various groundwater and soil contaminants including halogenated organics, heavy metals, nitrates, arsenate and pesticides [1]. However, compared to chlorinated aliphatics, chlorinated aromatics are generally recalcitrant to ZVI dechlorination since the C–Cl bond in the aromatic ring has much higher bond strength [2].

To enhance the reactivity and functionality of ZVI, depositing a second metal such as Ni, Cu, Pt or Pd as a catalyst onto the iron surface leads to the synthesis of bimetallic iron particles. As one of the noble metals, Pd can utilize the produced H_2 from ZVI corrosion and accelerate the rates of dechlorination reaction [3,4]. Besides, Pd can serve as the cathode to accelerate electron transfer from ZVI and leads to the improvement of dechlorination reactions [5]. The activity of ZVI can be also enhanced by decreasing its particle size [6]. Compared to the micro-scale counterparts, iron nanoparticles have much higher dechlorination reactivity, attributing to the extraordinary large specific surface area [7].

Chlorophenols (CPs) constitute a particular group of priority toxic chlorinated pollutants listed by the US EPA, because most of them are toxic, biorefractory and difficult to degrade in the natural environment. Due to their broad-spectrum antimicrobial properties, CPs have been used as preservative agents for wood, paints, vegetable fibers and leather and as disinfectants. In addition, they have been widely employed in the manufacturing of herbicides, fungicides, pesticides, insecticides, pharmaceuticals and dyes and may be also generated as by-products during waste incineration, the bleaching of pulp with chlorine, and in the dechlorination of drinking water [8]. As a result, CPs can be detected in soil, groundwater, and even in the food chains [9]. Particularly, 2,4,6-trichlorophenol and 2,4-dichlorophenol are listed in the Drinking Water Contaminant Candidate List (CCL) of US EPA and their limiting permissible concentration in drinking water should not exceed 10 $\mu g\,L^{-1}$ [10].Unlike chlorinated aliphatics, chlorinated aromatics are difficult to be dechlorinated via electrophilic addition. Therefore, hydrodechlorination of these aromatics via hydrogen addition catalyzed by the noble metals of the bimetallic iron particles is pursued. In the past decade, there were a few studies investigating the dechlorination characteristic of chlorophenols in bimetallic systems [3,11–13]. The study by Kim and Carrway [12] revealed that the microscale bimetals exhibited very weak reactivity toward dechlorination of pentachlorophenol. However, other researchers have reported that 2,4-dichlorophenol could be successfully hydrodechlorinated by bimetallic Pd/Fe [11,13], especially when the bimetal was of nano-size [3].

In this study, to gain insight into the role of particle size and the role of catalyst for CPs hydrodechlorination, Pd/Fe nanopar-

* Corresponding author. Tel.: +65 67906933; fax: +65 67910676.
E-mail address: cttlim@ntu.edu.sg (T.-T. Lim).

1383-5866/$ – see front matter © 2010 Elsevier B.V. All rights reserved.
doi:10.1016/j.seppur.2010.10.010

ticles were synthesized. Three CPs, i.e. 4-chlorophenol (4CP), 2,4-dichlorophenol (24DCP), and 2,4,6-trichlorophenol (246TCP) were chosen for investigation of their reductive dechlorination characteristics with the Pd/Fe. The experiments were designed in order to identify the reactive sites involved in the CPs dechlorination and the governing factors such as pH, temperature, catalyst loading and hydrogen evolution. Attempt to model the consecutive dechlorination of CPs into phenol was carried out to identify the major pathways and to understand the influence of molecular structure on selectivity by the reactive sites in the CPs dechlorination process.

2. Experimental

2.1. Chemicals

4-Chlorophenol (4CP), 2,4-dichlorophenol (24DCP), 2,4,6-trichlorophenol (246TCP), 2-chlorophenol (2CP), 2,6-dichlorophenol (26DCP), sodium borohydride ($NaBH_4$), acetone and iron powder (325 mesh, BET specific surface = $0.0786 \pm 0.0159\ m^2\ g^{-1}$) were obtained from Fisher Singapore. Phenol (Ph), $Pd(C_2H_3O_2)_2$, $FeSO_4{\cdot}7H_2O$, $NiSO_4$, $CuSO_4$, $CoCl_2$ and $PtCl_2$ were purchased from Sigma–Aldrich Singapore. In this study, deoxygenated ultrapure water was used in all experiments.

2.2. Synthesis and characterization of the nanoscale Pd/Fe particles

Nanoscale ZVI particles were produced by reduction of ferrous salt with $NaBH_4$ according to the following reaction (1). Then the palladized iron nanoparticle was prepared by soaking the fresh ZVI particles in an acetone solution of palladium(II) acetate (reaction (2)).

$$Fe^{2+} + 2BH_4^- + 6H_2O \rightarrow Fe^0\downarrow + 2B(OH)_3 + 7H_2\uparrow \quad (1)$$

$$Pd^{2+} + Fe^0 \rightarrow Pd\downarrow + Fe^{2+} \quad (2)$$

In order to avoid oxidation, palladized iron nanoparticles were prepared freshly before all experiments. The typical synthesized procedure in the present study is depicted as follows: predetermined volume of $FeSO_4{\cdot}7H_2O$ solution was added to 38 mL serum bottle (i.e. Fe content of $5\ g\ L^{-1}$). Prior to the synthesis, the solution pH was adjusted at 6.5 to precipitate $Fe(OH)_2$ [14]. Then a slight stoichiometric excess of $NaBH_4$ solution was added dropwise, resulting in the formation of iron nanoparticles. After washing with deoxygenated water for several times, the fresh ZVI nanoparticles were soaked with appropriate amount of palladium (II) acetate in acetone solution. After rigorous mixing, Pd/Fe nanoparticles were produced and rinsed to remove the residual acetone.

Prior to the characterization, all synthesized Pd/Fe nanoparticles were dried under argon purging and then sealed under argon atmosphere to avoid oxidation. Brunauer–Emmett–Teller (BET) specific surface area of the synthesized nanoscale Pd/Fe particles was measured using nitrogen adsorption method with a surface analyzer (Micromeritics Instrument Corp., Norcross, GA). Before the analysis, the particles were dried in vacuum at 25 °C for 24 h and then under a flow of hydrogen at 260 °C for 4 h. Transmission electron microscope (TEM) images of the particles were obtained with a JEM 2010 microscope (Philips Electronics Co., Eindhoven, Netherlands) performed at a voltage of 200 kV. Scanning electron microscope (SEM) images were obtained through a microscope (Stereoscan 420, Leica, Cambridge Instruments, UK). X-ray diffraction (XRD) analysis was performed by using Bruker AXS D8 advanced X-ray diffractometer ($\lambda = 1.5418$ Å). X-ray photoelectron spectrometry (XPS) analysis was performed by a PHI 5600 XPS system, with Mg anode X-ray source, operated at a power of 300 W.

2.3. Experimental procedure

Batch dechlorination experiments of 4CP, 24DCP, and 246TCP were carried out. Before the dechlorination experiments, each 38 mL serum bottle containing a pre-determined amount of 0.5% Pd/Fe fresh particles was added with the deoxygenated stock solution of CPs at $20\ mg\ L^{-1}$ until no headspace was left. Multiple bottles were prepared in each run of the batch experiments. These bottles were capped with Teflon-lined rubber septa and aluminum caps and placed on an orbital shaker (200 rpm) at room temperature (25 ± 1 °C) in the dark. At each specific sampling time, one bottle was sacrificed and aqueous sample was withdrawn by a gastight syringe (Hamilton) with a 0.2 μm filter for analysis of the parent CPs, organic intermediates and chloride.

Comparison of dechlorination experiments by using different ZVI-based bimetals were conducted under similar conditions. Four bimetallic particles, i.e. Ni/Fe, Cu/Fe, Pt/Fe and Co/Fe were prepared similarly as that for Pd/Fe nanoparticles, except the catalyst metals used.

For the experiments of H_2 evolution, a series of serum bottles containing $5\ g\ L^{-1}$ nanoscale Pd/Fe (Pd loading ratio 0.5%) were prepared. 30 mL of $20\ mg\ L^{-1}$ 246TCP solution was added into each bottle under argon atmosphere resulting in 8 mL of argon-filled headspace. Then the bottles were immediately caped and placed on the orbital shaker (200 rpm) at room temperature (25 ± 1 °C) in the dark. At predetermined sampling intervals, one bottle was sacrificed and 2 mL of gas sample in the headspace was withdrawn for the analysis of H_2 concentration.

2.4. Sample analysis

The CPs concentrations were measured by HPLC [15]. Qualitative identification of the intermediates was performed with a gas chromatograph (Agilent 6890, USA) equipped with a $30\ m \times 0.25$ μm DB5 column and mass selective detector. Before GC/MS analysis, water samples were pre-extracted by dichloromethane. The GC/MS column temperature was programmed from 60 °C (held 2 min) to 285 °C (held 2 min) at a rate of $10\ °C\ min^{-1}$. Released chloride ions (Cl^-) was measured by IC (Shimadzu, Singapore) coupled with a Shim-Pack IC-A3 column (4.6 mm × 150 mm) and a conductivity detector. The produced hydrogen gas was analyzed by a micro-gas chromatograph (Varian 4900, USA) equipped with a thermal conductivity detector. A Molsieve 5A Plot column was used with argon as carrier gas at 60 °C.

3. Results and discussion

3.1. Characterization of Pd/Fe nanoparticles

The BET specific surface area of the synthesized Pd/Fe nanoparticles was $26\ m^2/g$. The SEM and TEM images of the fresh Pd/Fe nanoparticles and the reacted (after 7 d) Pd/Fe nanoparticles are shown in Fig. 1. The freshly prepared Pd/Fe nanoparticles, with particle size ranging from 10 to 100 nm, appeared to aggregate together (Fig. 1c). After 7 d of reaction, the platelet-shaped crystals appeared (Fig. 1b), suggesting the formation of iron oxides resulting from iron corrosion in water. These minerals were likely composed of goethite (α-FeOOH) or lepidocrocite (γ-FeOOH) [16,17]. Huang and Zhang [17] also suggested that a stratified ZVI corrosion coating would form in water, for which the outer and middle layers comprised both FeOOH and Fe_3O_4, while the inner layer mainly consisted of Fe_3O_4. This is generally consistent with our observation in XPS spectra and XRD patterns. Fig. 1e shows the XRD patterns of the fresh and the 7 d aged Pd/Fe sample. The XRD pattern for the fresh sample presents a strong peak peaks 44.66° which cor-

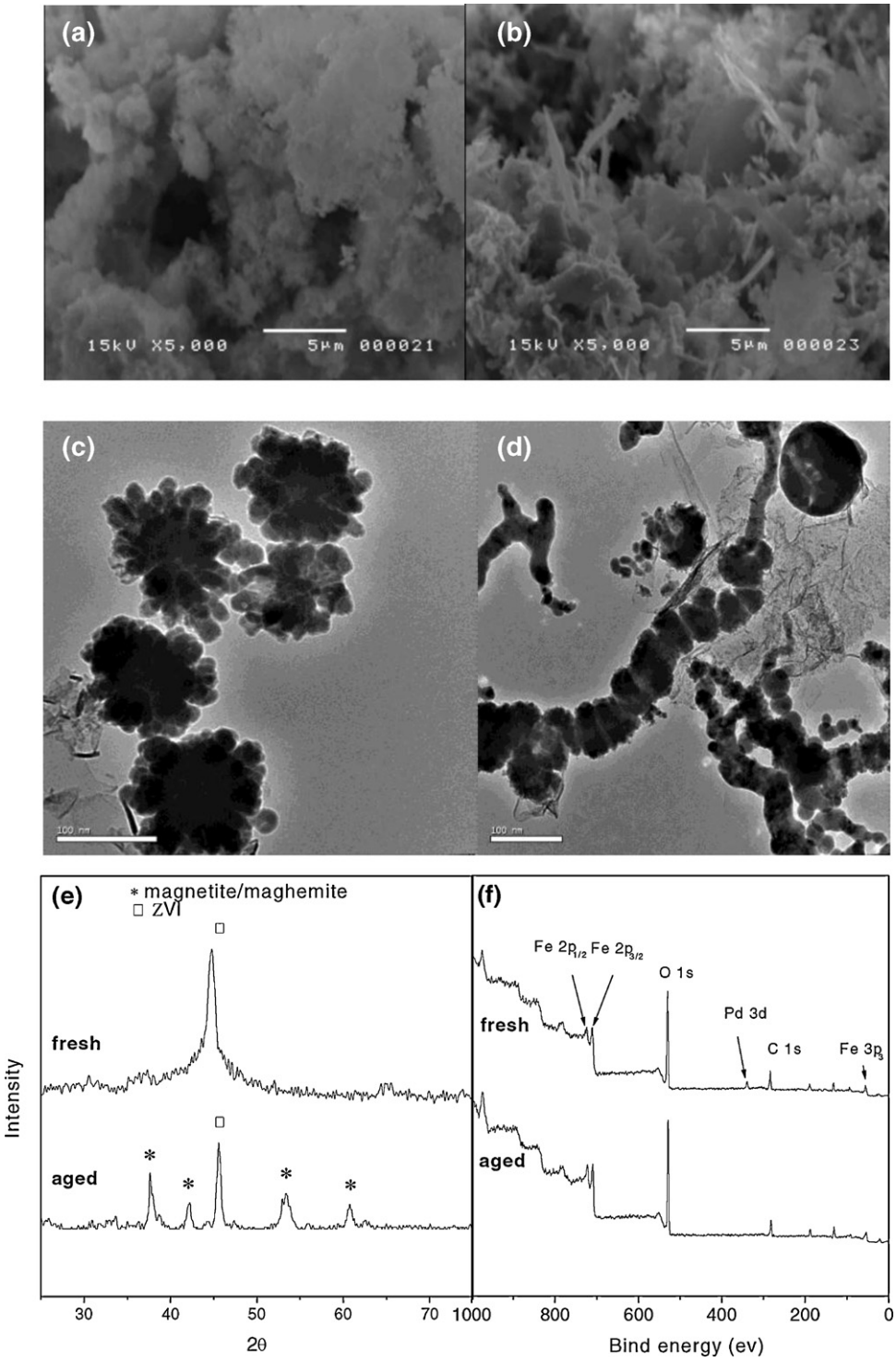

Fig. 1. (a) SEM image of fresh Pd/Fe nanoparticles, (b) SEM image of aged Pd/Fe nanoparticles (7 d), (c) TEM image of fresh Pd/Fe nanoparticles, (d) TEM image of aged Pd/Fe nanoparticles, (e) XRD patterns of fresh and aged Pd/Fe nanoparticles and (f) XPS spectra of fresh and aged Pd/Fe nanoparticles.

responds to the body-centered cubic N–Fe^0 at the (1 1 0) plane. The peaks in the XRD pattern of the aged sample show evidence of iron oxides, possibly Fe_3O_4 (magnetite) or Fe_2O_3 (maghemite), or their mixture. This agrees with the fact that Fe^0/Fe_3O_4 couple is more thermodynamically favorable at pH above 6.1 [18]. The XPS survey scan (Fig. 1f) shows the presence of Fe and Pd over the surface of the fresh Pd/Fe sample. The Fe 2p spectra of the fresh and aged samples show similar characteristic peaks with binding energies of 724.7 eV for Fe 2p1/2 and 710.9 eV for Fe 2p3/2, which are assigned to the oxidized iron, indicating that the surface of ZVI was covered by a layer of oxide film which might be formed during the drying process. For the 7 d aged sample, the chemical state of Pd could not be identified, which might be due to its coverage by iron oxides formed. It also implies that ZVI core shrank and concomitantly thickness of the iron oxides shell increased after reaction. The atomic ratios of ZVI to the oxidized iron were 1:1 and 1:2 with respect to fresh and aged samples, respectively. This indicates the core/shell structure of the Pd/Fe

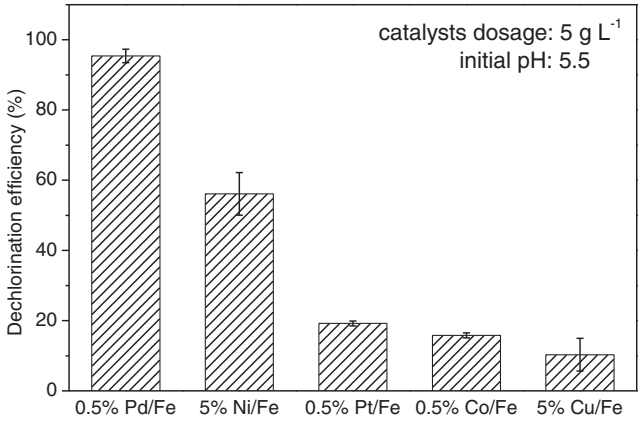

Fig. 2. Dechlorination of 246TCP with different bimetallic nanoparticles.

particles, with iron oxide in the outer of the sphere and ZVI in the inner.

3.2. Dechlorination of CPs with Pd/Fe nanoparticles

3.2.1. 246TCP dechlorination with microscale Pd/Fe and different bimetallic nanoparticles

Depositing 0.5% (w/w) Pd on the commercial ZVI particles (microscale) could not lead to an ideal dechlorination of 246TCP. With 50 g L^{-1} of microscale Pd/Fe dosage adopted, only 9.1% of 246TCP was dechlorinated after 24 h of reaction (data no shown). The $t_{1/2}$ for the pseudo-first-order dechlorination of 246TCP by the microscale Pd/Fe was 43 d. The low dechlorination rate might attribute to the low specific surface area of the microscale Pd/Fe.

The dechlorinations of 246TCP by five different bimetallic nanoparticles, i.e. Pd/Fe, Ni/Fe, Pt/Fe, Co/Fe and Cu/Fe, were also compared (Fig. 2). It is obvious that Pd/Fe could dechlorinate 94% of 246TCP within 1 h of reaction, while Ni/Fe could dechlorinate 56% of 246TCP. Pt/Fe, Co/Fe and Cu/Fe achieved dechlorianation efficiencies of less than 20%. Thus, Pd/Fe appeared to be the most reactive with respect to CPs dechlorination.

3.2.2. Kinetic modeling of the three CPs dechlorination by Pd/Fe nanoparticles

It is well established that the pseudo-first-order kinetics could be applied in the reductive dechlorination of chlorinated organics by the bimetallics nanoparticles [3]. Therefore, the pseudo-first-order reaction kinetics was adopted to model all the dechlorination reactions of the three CPs (4CP, 24DCP, 246TCP) by Pd/Fe nanoparticles.

Fig. 3 shows all the hypothetical transformation pathways of 4CP, 24DCP and 246TCP dechlorination with Pd/Fe nanoparticles, respectively. The corresponding sets of first-order kinetic equations are expressed as follows.

For 4CP as the parent compound:

$$\frac{dC_{4CP}}{dt} = -k_{1,4CP}C_{4CP} \quad (3a)$$

For 24DCP as the parent compound:

$$\frac{dC_{24DCP}}{dt} = -(k_{1,24DCP} + k_{2,24DCP})C_{24DCP} \quad (4a)$$

$$\frac{dC_{2CP}}{dt} = k_{1,24DCP}C_{24DCP} - k_{3,24DCP}C_{2CP} \quad (4b)$$

$$\frac{dC_{4CP}}{dt} = k_{2,24DCP}C_{24DCP} - k_{4,24DCP}C_{4CP} \quad (4c)$$

$$\frac{dC_{Ph}}{dt} = k_{3,24DCP}C_{2CP} + k_{4,24DCP}C_{4CP} \quad (4d)$$

Table 1
Kinetic constants of three CPs dechlorinated by the Pd/Fe nanoparticles.

Rate constants	Parent compounds		
	4CP	24DCP	246TCP
Observed			
k_{obs} (10^{-3} min^{-1})[a]	231	74.4	51.8
k_{SA} (10^{-3} L min^{-1} m^{-2})[b]	1.78	0.57	0.40
k_{Pd} (L min^{-1} g^{-1})[c]	9.24	2.98	2.07
$t_{1/2}$ (min)[d]	2.39	8.38	14.5
R^2[e]	0.992	0.981	0.991

[a] k_{obs} stands for pseudo-first-order dechlorination kinetic rate constant for degradation of the parent CPs.
[b] k_{SA} is specific dechlorination rate constant; $k_{SA} = k_{obs}/\rho_a$, where ρ_a is the specific surface area of the nanoscale particles (m^2 L^{-1}).
[c] k_{Pd} represents the k_{obs} normalized by the Pd loading.
[d] $t_{1/2}$ is the half-life period (min) of the parent CPs.
[e] R^2 is coefficient of determination from the overall regression analysis.

For 246TCP as the parent compound:

$$\frac{dC_{246TCP}}{dt} = -(k_{1,246TCP} + k_{2,246TCP})C_{246TCP} \quad (5a)$$

$$\frac{dC_{24DCP}}{dt} = k_{1,246TCP}C_{246TCP} - (k_{3,246TCP} + k_{5,246TCP})C_{24DCP} \quad (5b)$$

$$\frac{dC_{26DCP}}{dt} = k_{2,246TCP}C_{246TCP} - k_{4,246TCP}C_{26DCP} \quad (5c)$$

$$\frac{dC_{2CP}}{dt} = k_{4,246TCP}C_{246TCP} + k_{5,246TCP}C_{24DCP} - k_{7,246TCP}C_{2CP} \quad (5d)$$

$$\frac{dC_{4CP}}{dt} = k_{3,246TCP}C_{246TCP} - k_{6,246TCP}C_{4CP} \quad (5e)$$

$$\frac{dC_{Ph}}{dt} = k_{6,246TCP}C_{246TCP} + k_{7,246TCP}C_{2CP} \quad (5f)$$

where k_n represent rate constants shown in Fig. 3 and only correspond to the specific pathway according to the different parent CPs, C denotes concentration of the compound shown in its subscript. These rate equations can be solved and the solutions are presented in Appendix A.

3.2.3. Dechlorination of 4CP, 24DCP and 246TCP with Pd/Fe nanoparticles

The results of 4CP, 24DCP and 246TCP dechlorination with 0.5% (w/w) Pd/Fe nanoparticles at 5 g L^{-1} are shown in Fig. 4. The carbon mass balances were consistently achieved throughout all experiments (Fig. 4a–c), which indicated very low adsorption of CPs on the Pd/Fe nanoparticle surface or the container, unlike the Pd/Fe hydrodechlorination of chlorinated ethanes [19].

Table 1 summarizes the observed dechlorination rate constants of three CPs and the calculated k_n values by fitting the experimental data and kinetic models using non-linear least square regression analysis. The fitted curves are shown in Fig. 4a–c. According to the k_{SA} values of the three CPs, the order of CPs degradability with Pd/Fe nanoparticles is 246TCP < 24DCP < 4CP. The result is consistent with the observation that increasing the halogenated number of polyhaloaromatics would decrease the hydrodehalogenation rate in the Pd–H_2 system [4]. It can also be reflected by the initial rates of chloride releases during dechlorination of the three CPs by Pd/Fe nanoprticles, as shown in Fig. 4d. Therefore, the increased number of chlorines in the benzene ring would hinder the dechlorination process and C–Cl bond scission. Ph was detected as the only end product. Apparently, the catalytic hydrogenation by Pd/Fe nanoparticles could not overcome the resonance energy of the benzene ring.

The 24DCP could be hydrodechlorinated following two different pathways, i.e. 24DCP → 2CP → Ph and 24DCP → 4CP → Ph.

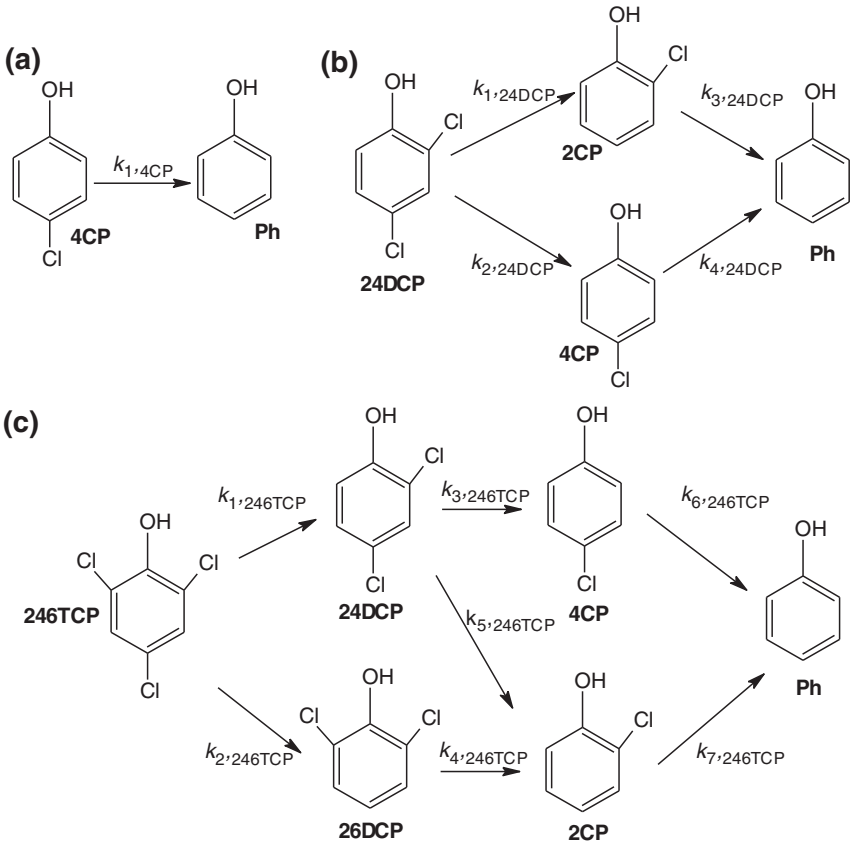

Fig. 3. Possible reaction pathways for the dechlorination of (a) 4CP, (b) 24DCP and (c) 246TCP with Pd/Fe nanoparticles.

By fitting the experimental data of 24DCP dechlorination reaction with kinetic model (Fig. 3b), the derived k_n values can be calculated as: $k_{1,24DCP} = 0.0449\ min^{-1}$, $k_{2,24DCP} = 0.0286\ min^{-1}$, $k_{3,24DCP} = 0.0869\ min^{-1}$, $k_{4,24DCP} = 0.1929\ min^{-1}$. Due to $k_{1,24DCP} > k_{2,24DCP}$, it indicated that hydrodechlorination of chlorine in *ortho*-position is more favorable when 24DCP is dechlorinated to monochlorophenols by Pd/Fe nanoparticles.

Fig. 4c presents the reductive dechlorination of 246TCP with Pd/Fe nanoparticles. The initial 246TCP molecules could be almost completely dechlorinated within 1 h of reaction. Since 26DCP was not detected throughout the dechlorination experiments, 24DCP could be identified as the sole DCP intermediate. Therefore, the derived k_n values can be determined as: $k_{1,246TCP} = 0.0518\ min^{-1}$, $k_{2,246TCP} = 0\ min^{-1}$, $k_{3,246TCP} = 0.0249\ min^{-1}$, $k_{4,246TCP} = 0\ min^{-1}$, $k_{5,246TCP} = 0.0387\ min^{-1}$, $k_{6,246TCP}$ =0.0425, $k_{7,246TCP} = 0.1117\ min^{-1}$. The result suggested that chlorine in the *meta* position of –OH on the ring is easier to be substituted during the hydrodechlorination of 246TCP.

3.2.4. Factors affecting 246TCP dechlorination by Pd/Fe nanoparticles

The linear correlation between the initial catalyst dosage of Pd/Fe nanoparticles and 246TCP dechlorination rate constants (k_{obs}) was evident (Fig. 5a). With increasing Pd/Fe nanoparticles loading, k_{obs} increases. Apparently, it can be attributed to the increase of total Pd catalyst surface area taking part in the 246TCP dechlorination reaction. Nevertheless, when normalized with the surface area of using nanoparticles, the obtained values of k_{SA} (specific dechlorination rate constant) are relatively constant, indicating that the dechlorination rate of 246TCP was closely related to the Pd site on ZVI surface.

The linear relationship between Pd loading in the nanoparticles and k_{obs} was observed (Fig. 5b). Dechlorination of 246TCP was not found when Pd loading was zero. It is obvious that Pd was the exclusive reactive site on the surface of Pd/Fe nanoparticles. Therefore, it can be concluded that hydrodechlorination of the CPs is surface-mediated and only occurred on Pd site of the nanoparticles. The role of Pd in the hydrodechlorination reactions will be further discussed in Section 3.4.

The degradation enhancement at elevated temperatures can be revealed by analyzing the temperature-dependent reaction rates:

$$\ln k_{obs} = \frac{A}{RT} E_a \quad (6)$$

where A is a constant, E_a is the activation energy ($kJ\ mol^{-1}$), R is the universal gas constant ($8.314\ J\ K^{-1}\ mol^{-1}$), and T is the absolute temperature (K). It is well known that surface-mediated reactions usually involves several steps in the overall reaction mechanism including the diffusion of a reactant to the surface, a chemical reaction on the surface, and the diffusion of a product back into the bulk solution. The slowest reaction step or the rate-limiting step governs the overall reaction kinetics. Previous studies reported that dechlorination reactions controlled by mass transfer have a low experimentally observed E_a value of typically 10–20 $kJ\ mol^{-1}$ [20]. In the present study, E_a value was 29.8 $kJ\ mol^{-1}$ for the 246TCP dechlorination by Pd/Fe nanoparticles, as determined from the linear plot of Arrhenius equation (Fig. 5c). It can therefore be concluded that that a surface chemical reaction instead of mass transfer is the controlling step in the overall process kinetics.

The reaction pH is considered to affect the COCs dechlorination with ZVI or bimetals, due to the different corrosion reactions of iron in acidic and alkaline solutions as given below:

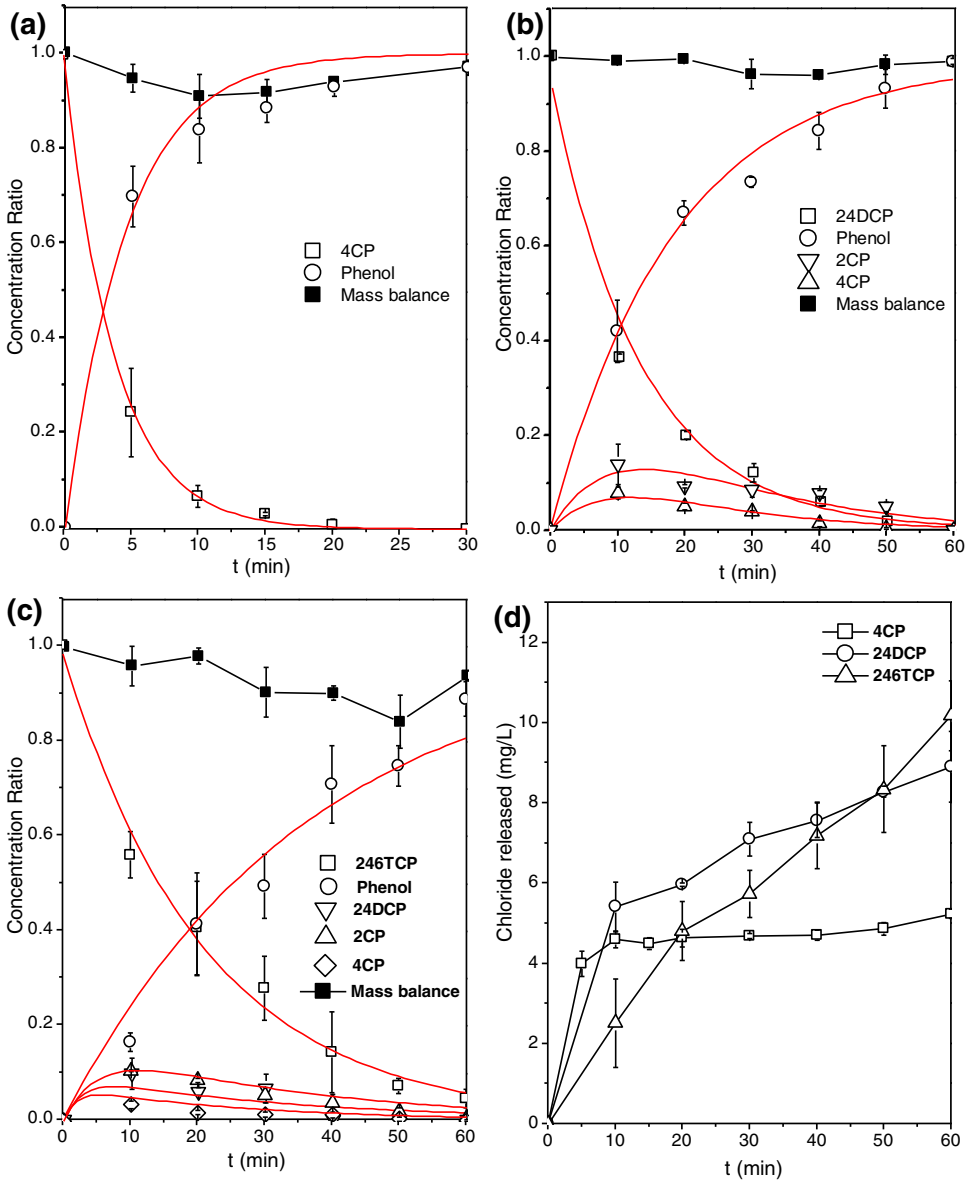

Fig. 4. Dechlorination of CPs in 0.5% Pd/Fe nanoparticles at 5 g L^{-1} (a) 4CP, (b) 24DCP, (c) 246TCP and (d) chloride released in the 3 systems. The initial CPs concentration is 20 mg L^{-1} and pH is 5.5. Error bars represent 95% confidence limits.

Acidic condition:

$$Fe^0 + 2H^+ \rightarrow Fe^{2+} + H^2\uparrow \quad (7)$$

Alkaline condition:

$$Fe^0 + 2H_2O \rightarrow Fe^{2+} + 2OH^- + H_2\uparrow \quad (8)$$

Besides, deactivation of ZVI or ZVI-based bimetals should be also of concern in solutions of different pH. In acidic solution, loss dislodgement of Pd islets on ZVI surface occurs as a result of erosion of the underlying ZVI, while surface passivation by iron hydroxide precipitation occurs at pH > 5.6. In addition, extensive H_2 gas formation may produce a blanket of gas bubbles around the catalyst surface and temporarily deactivate the catalyst [21]. Fig. 5d indicated that solution pH had a significant influence on the 246TCP dechlorination with Pd/Fe nanoparticles. Compared to the rapid dechlorination of 246TCP in the natural solution (initial pH = 5.5), there were strong inhibitions of 246TCP dechlorination observed in the alkaline solution (e.g. initial pH = 10.0), and slight inhibitions observed in the acidic condition (e.g. initial pH = 3.0). In addition, the interaction of ZVI and water generally leads to elevation of pH since the corrosion of iron resulted in release of OH^-. During the dechlorination reactions, with initial alkaline condition, it was observed that the change in pH value was rather insignificant. However, under initial acidic conditions, pH value rapidly increased to 7.0, and then reach equilibrium at 8.0–8.5 till the end of reaction.

The pH effect might be attributed to the participation of protons during the dechlorination reaction. In the acidic condition, the intensive iron corrosion led to dislodgement of Pd from the particle surface and production of large quantity of H_2. Both phenomena decreased the dechlorination reaction rate due to the loss of the sole reactive site of Pd/Fe and formation of H_2 gas barrier to mass transfer. While in the alkaline solution, slow production of H_2 limits the dechlorination reaction, and precipitation of metal hydroxides could also form passivating layers on the catalyst surface and deactivate the Pd/Fe bimetallic nanoparticles.

3.3. H_2 evolution with Pd/Fe nanoparticles

Fig. 6 shows cumulative H_2 gas formation during 246TCP dechlorination with 0.5% Pd/Fe nanoparticles at 5 g L^{-1}. It can be seen that

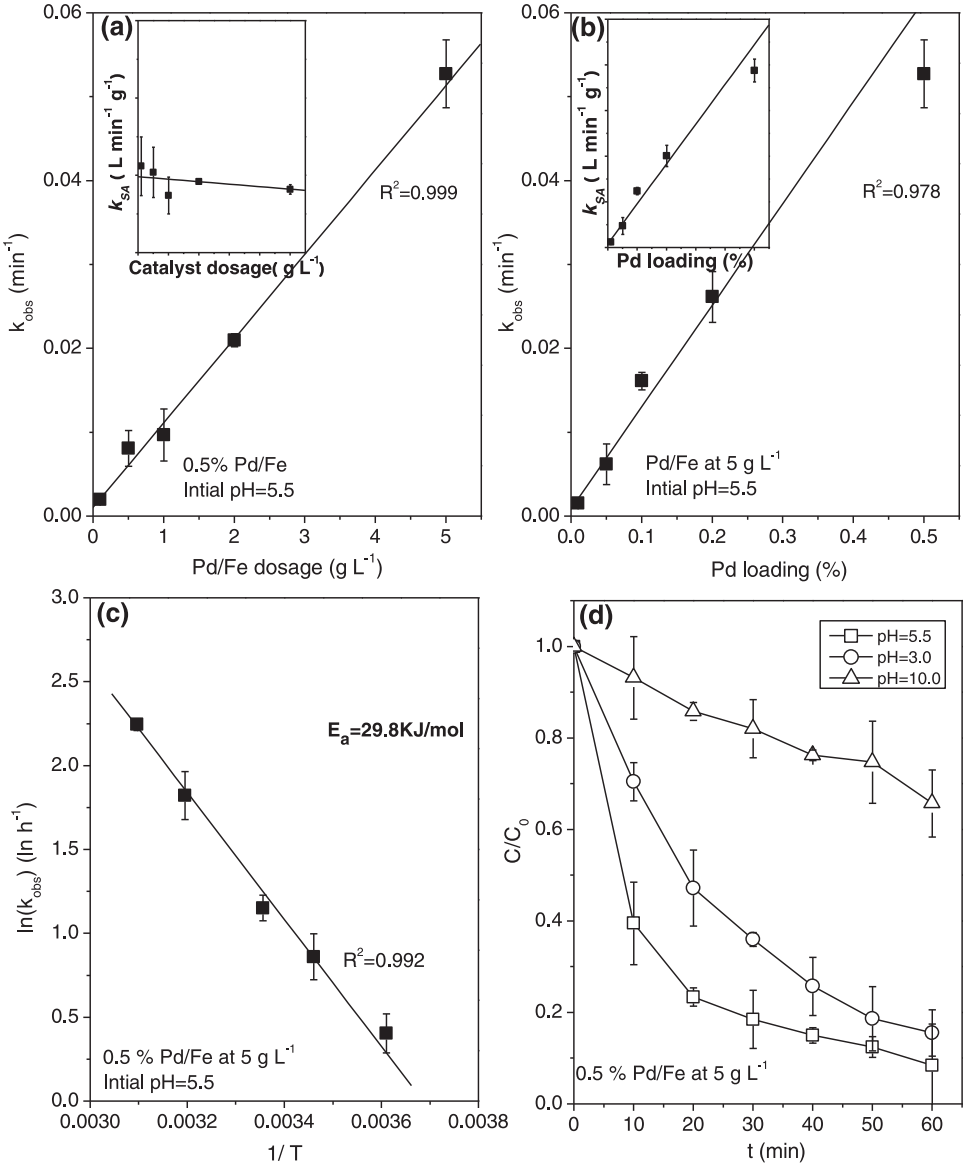

Fig. 5. Effect of (a) Pd/Fe dosage, (b) Pd loading ratio in Pd/Fe, (c) reaction temperature and (d) initial pH on the 246TCP dechlorination rates with Pd/Fe nanoparticles. Error bars represent 95% confidence limits.

H_2 was rapidly accumulated within the initial reaction period and H_2 amounted to 1.74 mmol at 1 h reaction time. As shown in the inset of Fig. 6, the H_2 accumulation could be approximately fitted by the pseudo first-order kinetics ($k = 0.19\ h^{-1}$) in initial reaction period from 0 to 5 h, while it reached a steady rate and approximately followed the zero-order kinetics ($k = 1.37$ mmol d^{-1}) in the extended period of reaction (24–120 h). Generally, the H_2 production in ZVI/water systems highly depended on iron corrosion rate that was directly affected by ZVI content and solution pH. It has been reported that in the nZVI/water system the H_2 accumulation rate was rather constant regardless of the age of the particles [22]. Since the loss of Fe^0 content in the system could be well applied by the first-order kinetics at equilibrium pH [18], it can be concluded that the H_2 accumulation in the Pd/Fe–water system appeared to follow the first-order kinetic, after specified the observed zero-order kinetic by the iron age. The observed first-order accumulation of H_2 in the initial period might be attributed to negligible loss of iron.

3.4. Dechlorination mechanism of CPs in Pd/Fe bimetallic system

Regarding COCs dechlorination in ZVI/water system, three mechanisms: (a) direct reduction on fresh ZVI surface, (b) reduction by ferrous iron, and (c) reduction by H_2 through catalysis, have been proposed [23]. Meanwhile, with the deposition of a noble metal on ZVI surface, the bimetal/water system would have stronger reductive ability due to production of a new activated reductant, atomic hydrogen (H*). Since the hydrogen overpotential of Pd is much lower than that of iron metal, H_2 dissociation on Pd surface is easily catalyzed with a low activation barrier ($\leq$8.4 kJ mol^{-1}) [24]. In a typical Pd/Fe system, the production of H* may follow two routes—catalyzed decomposition of H_2 gas to H*, and electron abstraction by H^+, as shown in Fig. 7a. Aliphatic COCs can be not only hydrodechlorinated on Pd surface with H* but also directly reducted on the fresh ZVI surface via electron abstraction [19]. For chlorinated aromatics, however, the direct reduction by ZVI on its surface is insignificant

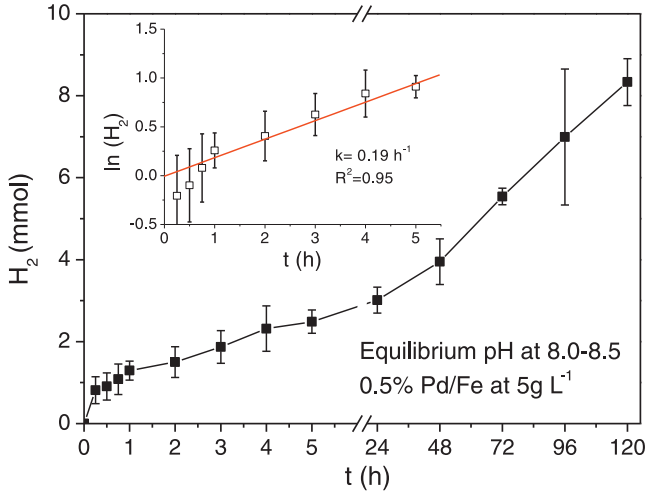

Fig. 6. Long-term H_2 evolution with Pd/Fe nanoparticles during the dechlorination of 246TCP. Error bars represent 95% confidence limits.

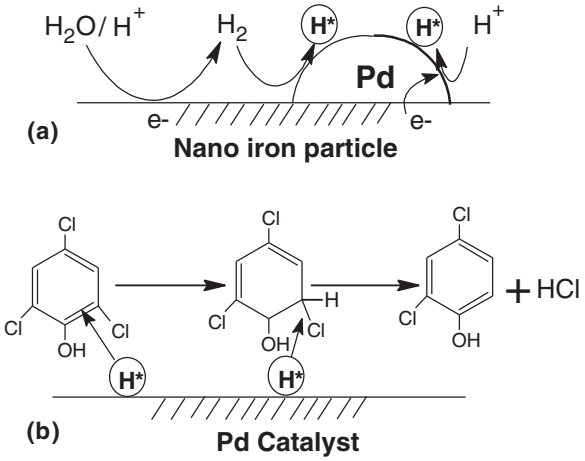

Fig. 7. Schematic of proposed catalytic hydrodechlorination mechanism of CPs over nanoscle Pd/Fe (a) production of atomic hydrogen and (b) surface-mediated hydrodechlorination of CPs on Pd surface.

and the Pd-catalyzed hydrodechlorination reactions is dominant [3].

Pd-catalyzed hydrodechlorination reactions in aqueous suspension are generally substance-structure dependent. It was reported that good structure-reactivity correlations for chlorinated alkanes hydrodechlorination were observed, while the hydrodechlorination rates of unsaturated COCs, such as chlorinated ethenes and aromatics did not follow the order of C–Cl bond strength [25,26]. Therefore, in the hydrodechlorination process, the addition of H* from Pd surface to unsaturated COCs, especially addition to the double bonds, seems to be rate-determining.

Fig. 7b illustrates a proposed hydrodechlorination mechanism of CPs (e.g. 246TCP) in the Pd/Fe bimetallic system, which is exclusively surface-mediated on Pd catalyst. The CPs could be dissociatively adsorbed with the formation of a surface σ-complex via the aromatic ring carbon with the highest electron density. The reactivity of electrophilic hydrogen addition to the aromatic ring of CPs is determined by the characteristics of molecular structure that govern their inductive, steric and resonance effects. Different substituents on the aromatic ring lead to different effects on the electrophilic hydrogen addition. Generally, the presence of hydroxyl group (–OH) on the aromatic ring can activate the ring for electrophilic attack by electron donation, while chlorine group (–Cl) deactivates the ring by reducing the electron density of the aromatic ring. The additional presence of –Cl on the ring can further render the entire chlorine component less susceptible to hydrogen attack, due to the lower electron density via more Cl atoms associated with the ring carbons, and thus leads to lower hydrodechlorination reactivity. The steric effect is also important on the scission of –Cl from the aromatic ring and the degree of hydrodechlorination is clearly inhibited with increasing Cl substitution. With respect to the chlorinated aromatic isomers, the hydrodehalogenation selectivity is nonetheless dependent on their nature and C–Cl cleavage is inhibited by substituents at the *ortho*-position, especially. However, resonance effect for hydrogen addition reactions on the ring of CPs appears to have a negligible role, since reactivity of *ortho*/*para* isomers cannot be linked to the *meta*-form [25].

Taking these effects together, with respect to 246TCP molecular structure, the *meta* position of –OH on the ring is easier to be attacked by H* and electrophilic H addition to the double bond of the benzene ring tends to occur in 1,2 position. The subsequent electrophilic H addition on C–Cl leads to the bond cleavage and formation of 24DCP. This may explain that 26DCP is not the favorable dechlorinated product of 246TCP due to the hydrodechlorination selectivity on the ring. Under continuous electrophilic H* addition, all the C–Cl bonds would be dissociated and phenol is the end product.

4. Conclusion

The Pd/Fe nanoparticles could transform CPs via surface-mediated catalytic hydrodechlorination, and Pd catalyst was the only reactive site. The Pd is more reactive than Ni, Pt, Co and Cu. The H_2 generated by iron corrosion can be catalyzed on the Pd surface to produce atomic hydrogen (H*) for the CPs dechlorination reaction. The CPs could be finally dechlorinated to phenol. The relative reaction rate of CPs (4CP > 24DCP > 246TCP) provides additional evidence that the increase of chlorination in the aromatic ring retards the hydrodechlorination rate. The circumneutral condition appears to be the most favorable to the dechlorination reaction.

Appendix A.

For 4CP, the solutions are listed as:

$$C_{4CP,t} = e^{-k_1 t} C_{4CP,0} \quad \text{(A.1a)}$$

$$C_{Ph,t} = (1 - e^{-k_1 t}) C_{4CP,0} \quad \text{(A.1b)}$$

where k_1 denotes kinetic constant of 4CP dechlorination reaction ($k_{1,4CP}$).

For 24DCP, the solutions are:

$$C_{24DCP,t} = e^{-(k'_1+k'_2)t} C_{24DCP,0} \quad \text{(A.2a)}$$

$$C_{2CP,t} = \frac{k'_1}{k'_3 - (k'_1 + k'_2)} \left[e^{-(k'_1+k'_2)t} - e^{-k'_3 t} \right] C_{24DCP,0} \quad \text{(A.2b)}$$

$$C_{4CP,t} = \frac{k'_2}{k'_4 - (k'_1 + k'_2)} \left[e^{-(k'_1+k'_2)t} - e^{-k'_4 t} \right] C_{24DCP,0} \quad \text{(A.2c)}$$

$$C_{Ph,t} = C_{24DCP,0} - C_{24DCP,t} - C_{2CP,t} - C_{4CP,t} \quad \text{(A.2d)}$$

where k'_n denote different kinetic constants during the 24DCP dechlorination ($k_{n,24DCP}$).

For 246TCP, the solutions are:

$$\alpha_{246TCP} = e^{-(k''_1+k''_2)t} \quad \text{(A.3a)}$$

$$\alpha_{24DCP} = \frac{k''_1}{(k''_3 + k''_5) - (k''_1 + k''_2)} (e^{-(k''_1+k''_2)t} - e^{-(k''_3+k''_5)t}) \quad \text{(A.3b)}$$

$$\alpha_{26DCP} = \frac{k''_2}{k''_4 - (k''_1 + k''_2)}(e^{-(k''_1+k''_2)t} - e^{-k''_4 t}) \quad (A.3c)$$

$$\alpha_{2CP} = \frac{k''_2 k''_4}{k''_4 - (k''_1 + k''_2)}\left[\frac{e^{-(k''_1+k''_2)t} - e^{-k''_7 t}}{k''_7 - (k''_1 + k''_2)} - \frac{e^{-k''_4 t} - e^{-k''_7 t}}{k''_7 - k''_4}\right] + \frac{k''_1 k''_5}{(k''_3 + k''_5) - (k''_1 + k''_2)}\left[\frac{e^{-(k''_1+k''_2)t} - e^{-k''_7 t}}{k''_7 - (k''_1 + k''_2)} - \frac{e^{-(k''_3+k''_5)t} - e^{-k''_7 t}}{k''_7 - (k''_3 + k''_5)}\right] \quad (A.3d)$$

$$\alpha_{4CP} = \frac{k''_1 k''_3}{(k''_3 + k''_5) - (k''_1 + k''_2)}\left[\frac{e^{-(k''_1+k''_2)t} - e^{-k''_6 t}}{k''_6 - (k''_1 + k''_2)} - \frac{e^{-(k''_3+k''_5)t} - e^{-k''_6 t}}{k''_6 - (k''_3 + k''_5)}\right] \quad (A.3e)$$

$$\alpha_{Ph} = 1 - \alpha_{246TCP} - \alpha_{24DCP} - \alpha_{24DCP} - \alpha_{2CP} - \alpha_{4CP} \quad (A.3f)$$

where α denotes molar fractions, e.g. $\alpha_{Ph} = C_{Ph,t}/C_{246TCP,0}$, k''_n denote different kinetic constants during the 246TCP dechlorination ($k_{n,246TCP}$).

The different k_n values were obtained by fitting the experimental data into the respective expressions. The principle of least-squares was used to minimize the model error: the sum of squared difference (s^2) between the model-predicted and the experimental molar fractions of various compounds.

$$s^2 = \sum_{i}^{NC}\sum_{j}^{ND}(\alpha_{ij} - \hat{\alpha}_{ij})^2 \quad (A.4)$$

where NC is number of compounds detected, ND is number of data points for each of these compounds, α_{ij} and $\hat{\alpha}_{ij}$ are respectively the experimental and model-predicted molar fractions of the compounds at different reaction times. A MATLAB program was compiled to obtain the smallest s^2 and the corresponding best-fitted k_n values.

References

[1] J.T. Nurmi, P.G. Tratnyek, V. Sarathy, D.R. Baer, J.E. Amonette, K. Pecher, C. Wang, J.C. Linehan, D.W. Matson, R. Leepenn, M.D. Driessen, Characterization and properties of metallic iron nanoparticles: spectroscopy, electrochemistry, and kinetics, Environ. Sci. Technol. 39 (2005) 1221–1230.

[2] B. Aikawa, R.C. Burk, B.B. Sithole, Catalytic hydrodechlorination of 1-chlorooctadecane, 9,10-dichlorostearic acid, and 12,14-dichlorodehydroabietic acid in supercritical carbon dioxide, Appl. Catal. B 43 (2003) 371–387.

[3] J. Wei, X. Xu, Y. Liu, D. Wang, Catalytic hydrodechlorination of 2,4-dichlorophenol over nanoscale Pd/Fe: reaction pathway and some experimental parameters, Water Res. 40 (2006) 348–354.

[4] G.V. Lowry, M. Reinhard, Pd-catalyzed TCE dechlorination in water: effect of $[H_2](aq)$ and H_2-utilizing competitive solutes on the TCE dechlorination rate and product distribution, Environ. Sci. Technol. 35 (2001) 696–702.

[5] D.W. Elliott, W. Zhang, Field assessment of nanoscale bimetallic particles for groundwater treatment, Environ. Sci. Technol. 35 (2001) 4922–4926.

[6] W.X. Zhang, C.B. Wang, H.L. Lien, Treatment of chlorinated organic contaminants with nanoscale bimetallic particles, Catal. Today 40 (1998) 387–395.

[7] S.M. Ponder, J.G. Darab, T.E. Mallouk, Remediation of Cr(VI) and Pb(II) aqueous solutions using supported, nanoscale zero-valent iron, Environ. Sci. Technol. 34 (2000) 2564–2569.

[8] M. Pera-Titus, V. García-Molina, M.A. Baños, J. Giménez, S. Esplugas, Degradation of chlorophenols by means of advanced oxidation processes: a general review, Appl. Catal. B: Environ. 47 (2004) 219–256.

[9] WHO, Chlorophenols Other Than Pentachlorophenol, Environmental Health Criteria 93, World Health Organization, 1989.

[10] USEPA, http://www.epa.gov/OGWDW/ccl/ccl2.html, 2005.

[11] Y Liu, F. Yang, P.L. Yue, G. Chen, Catalytic dechlorination of chlorophenols in water by palladium/iron, Water Res. 35 (2001) 1887–1890.

[12] Y.-H. Kim, E.R. Carrway, Dechlorination of pentachlorophenol by zero valent iron and modified zero valent irons, Environ. Sci. Technol. 34 (2000) 2014–2017.

[13] G. Yuan, M.A. Keane, Catalyst deactivation during the liquid phase hydrodechlorination of 2,4-dichlorophenol over supported Pd: influence of the support, Catal. Today 88 (2003) 27–36.

[14] S.M. Ponder, J.G. Darab, J. Bucher, D. Caulder, I. Craig, L. Davis, N. Edelstein, W. Lukens, H. Nitsche, T.E. Mallouk, Surface chemistry and electrochemistry of supported zerovalent iron nanoparticles in the remediation of aqueous metal contaminants, Chem. Mater. 13 (2001) 479–486.

[15] T. Zhou, Y. Li, J. Ji, F.-S. Wong, X. Lu, Oxidation of 4-chlorophenol in a heterogeneous zero valent iron/H_2O_2 Fenton-like system: kinetic, pathway and effect factors, Sep. Purif. Technol. 62 (2008) 551–558.

[16] D.H. Phillips, B. Gu, D.B. Watson, Y. Roh, L. Liang, S.Y. Lee, Performance evaluation of a zerovalent iron reactive barrier: mineralogical characteristics, Environ. Sci. Technol. 34 (2000) 4169–4176.

[17] Y.H. Huang, T.C. Zhang, Reduction of nitrobenzene and formation of corrosion coatings in zerovalent iron systems, Water Res. 40 (2006) 3075–3082.

[18] Y. Liu, G.V. Lowry, Effect of particle age (Fe^0 content) and solution pH on NZVI reactivity: H_2 evolution and TCE dechlorination, Environ. Sci. Technol. 40 (2006) 6085–6090.

[19] H.L. Lien, W.X. Zhang, Hydrodechlorination of chlorinated ethanes by nanoscale Pd/Fe bimetallic particles, J. Environ. Eng. ASCE 131 (2005) 4–10.

[20] C. Su, R.W. Puls, Kinetics of trichloroethene reduction by zerovalent iron and tin: pretreatment effect, apparent activation energy, and intermediate products, Environ. Sci. Technol. 33 (1999) 163–168.

[21] G. Jovanovic, P. Znidarsic-Plazl, P. Sakrittichai, K. Al-Khaldi, Dechlorination of *p*-chlorophenol in a microreactor with bimetallic Pd/Fe catalyst, Ind. Eng. Chem. Res. 44 (2005) 5099–5106.

[22] H. Song, E.R. Carraway, Catalytic hydrodechlorination of chlorinated ethenes by nanoscale zero-valent iron, Appl. Catal. B: Environ. 78 (2008) 53–60.

[23] T.T. Lim, B.W. Zhu, Practical applications of bimetallic nanoiron particles for reductive dehalogenation of haloorganics: prospects and challenges, in: K.M. Carvalho-Knighton, C.L. Geiger (Eds.), Environmental Applications of Nanoscale and Microscale Reactive Metal Particles, American Chemical Society, USA, 2009, pp. 245–261 (Chapter 14).

[24] J. Feng, T.-T. Lim, Pathways and kinetics of carbon tetrachloride and chloroform reductions by nano-scale Fe and Fe/Ni particles: comparison with commercial micro-scale Fe and Zn, Chemosphere 59 (2005) 1267–1277.

[25] M.A. Keane, Hydrodehalogenation of haloarenes over silica supported Pd and Ni: a consideration of catalytic activity/selectivity and haloarene reactivity, Appl. Catal. A 271 (2004) 109–118.

[26] K. Mackenzie, H. Frenzel, F.-D. Kopinke, Hydrodehalogenation of halogenated hydrocarbons in water with Pd catalysts: reaction rates and surface competition, Appl. Catal. B 63 (2006) 161–167.